ACS Catalysis

Research Article

pubs.acs.org/acscatalysis

Phenol Deoxygenation Mechanisms on Fe(110) and Pd(111)

Alyssa J. R. Hensley,[†] Yong Wang,[†,‡] and Jean-Sabin McEwen*[,†,§,∥]

[†]The Gene & Linda Voiland School of Chemical Engineering and Bioengineering, [§]Department of Physics and Astronomy, [∥]Department of Chemistry, Washington State University, Pullman, Washington 99164, United States

[‡]Pacific Northwest National Laboratory, Institute for Integrated Catalysis, Richland, Washington 99352, United States

Supporting Information

ABSTRACT: The catalytic deoxygenation of phenolic compounds has become a major area of interest in recent years because they are produced during the pyrolysis of lignin and are present in biofuels. Our previous work showed that a PdFe bimetallic catalyst was catalytically active for the deoxygenation of phenolics. To better understand and control the catalytic deoxygenation reaction of phenolics, the detailed surface reaction mechanisms are needed for phenol, a key intermediate in phenolic deoxygeantion. Here, we have examined five distinct reaction mechanisms for the deoxygenation of phenol on the Fe(110) and Pd(111) surfaces so as to identify the most likely deoxygenation mechanism on these surfaces. Our results show that the elementary phenol deoxygenation reaction step for each mechanism was highly endothermic on Pd(111), whereas the same mechanisms are exothermic on Fe(110). On the basis of the reaction energy studies, detailed mechanistic studies were performed on the Fe(110) surface, and it was found that the most energetically and kinetically favorable reaction mechanism occurs via the direct cleavage of the C−O bond.

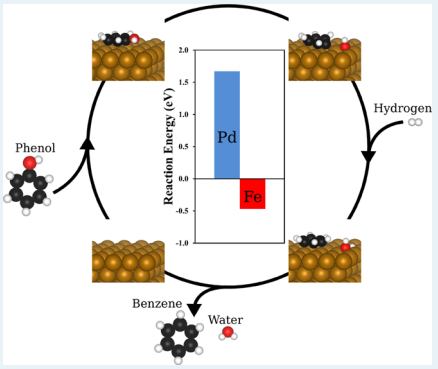

KEYWORDS: *Density Functional Theory, Minimum Energy Pathways, Transition State Theory, Phenol Deoxygenation, Fe(110), Pd(111), Benzene Production, BEP Relations*

1. INTRODUCTION

The catalytic hydrodeoxygenation (HDO) of phenolic compounds has become a major area of interest in recent years because of the increased need to find a sustainable energy replacement for fossil fuels.[1] Bio-oils produced via the fast pyrolysis of lignocellulosic biomass have a high potential for replacing traditional fossil fuels.[2] However, degradation of lignin, which accounts for ∼17 to 35 wt % of the lignocellulosic biomass, produces a significant amount of oxygen-containing phenolic compounds.[2−4] These oxygen-containing compounds have significant, negative effects on the application of bio-oils as fuel; namely, these compounds lower the fuels' heating value, decrease its stability, and produce fuel with a poor volatility and high viscosity.[5,6] Therefore, before these bio-oils can be used as a fuel, the oils must be further upgraded to remove the oxygen. In this work, we focus on the catalytic upgrading of phenolic compounds such as those produced via the degradation of lignin.

Thus far, hydrotreating in the form of catalytic HDO has been identified as the most attractive method for the upgrading of bio-oil.[2] To better understand and control the catalytic HDO reaction, the detailed reaction mechanism must be identified to better tailor catalysts for the removal of oxygen from phenolic compounds. The possible HDO mechanisms have been identified as being one of three reaction types: hydrogenation,[7−12] direct deoxygenation,[7,8,13,14] and tautomerization followed by deoxygenation of the aromatic species.[8,15−17]

The first HDO mechanism presented is the hydrogenation mechanism, which entails the hydrogenation of the phenolic compound to an equivalent cyclic, oxygenated alkane followed by deoxygenation. The remaining cyclic hydrocarbon is then either dehydrogenated to form an equivalent, deoxygenated aromatic compound (toluene for *m*-cresol, benzene for phenol, etc.)[7,8,12] or hydrogenated to a cyclohexane compound.[9−11] This mechanism has been primarily proposed for bifunctional catalyst systems that have a metal site to hydrogenate the aromatic ring and an acid site to cleave the C−O bond and dehydrogenate the compound to form the deoxygenated products.[9−11] The hydrogenation of the aromatic ring in the phenolic compound likely weakens the C−O bond, resulting in a reasonably low activation energy barrier for the deoxygenation reaction. However, this mechanism requires a large amount of hydrogen to proceed which can be costly.

An alternative mechanism to the hydrogenation mechanism is the direct deoxygenation mechanism.[7,8,13,14] This mechanism proceeds via the direct cleavage of the C−O bond in the phenolic compound, followed by the hydrogenation of the aromatic compound to form the deoxygenated reaction products. The benefit of this reaction mechanism over the hydrogenation mechanism is in the significant decrease in the

Received: September 16, 2014
Revised: November 27, 2014
Published: December 2, 2014

Scheme 1. Possible Deoxygenation Reaction Mechanisms for Phenol on a Metal Catalyst Surface (denoted by M)

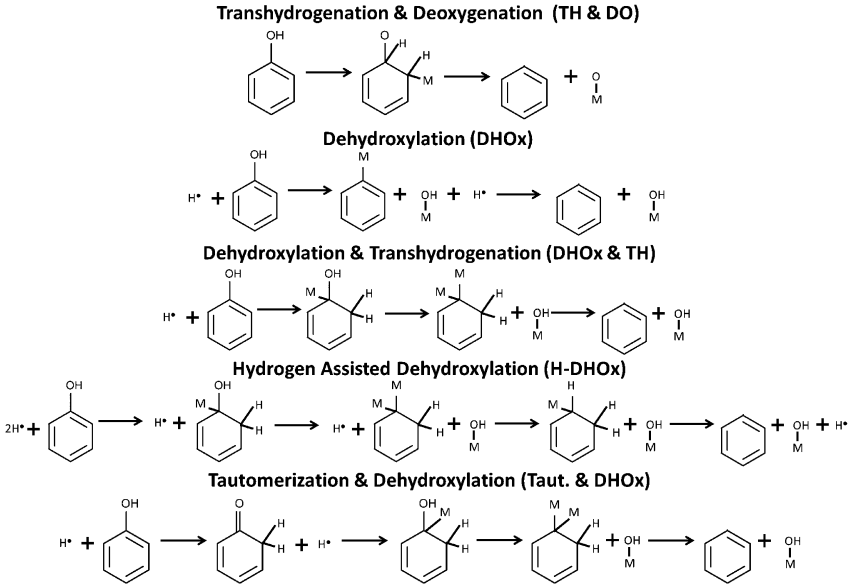

amount of hydrogen required to perform the HDO reaction; however, it has been suggested that the C−O cleavage reaction step requires high operating temperatures.[15] Clearly, further work in this area is necessary to determine the overall feasibility of this mechanism.

Recent work performed by Nie et al.[15] on the conversion of *m*-cresol has proposed that the improved reaction selectivity of their NiFe bimetallic catalyst is due to the vertical adsorption preference of *m*-cresol through the oxygen functional group. The vertical adsorption of the phenolic compound is then proposed to undergo a tautomerization reaction to the phenolic compound's equivalent ketone, followed by hydrogenation of the oxygen group and the oxygen-bonded ring carbon and then dehydrated to form the equivalent deoxygenated aromatic product. Further study by Nie et al.[16] showed that the HDO of *m*-cresol over Pt/SiO_2 catalysts likely occurs with the same initial tautomerization mechanism. A similar mechanism involving tautomerization reactions was presented by Kim et al. for the HDO of chloropyridinols.[17] The tautomerization reaction mechanism via the vertical adsorption of the phenolic compound is theorized to account for the bimetallic catalyst's improved HDO performance because this mechanism, through vertically adsorbed phenolics, is believed to limit ring hydrogenation and C−C bond cleavage reactions by reducing the aromatic ring to surface interactions.[15]

Under these three HDO reaction types, we have identified five possible deoxygenation mechanisms for the conversion of phenol to benzene that could potentially occur on the metal surface. These mechanisms are shown in Scheme 1.

The reactions presented in Scheme 1 were examined on the Fe(110) and Pd(111) surfaces via the adsorption of phenol through the aromatic ring (horizontal). In addition to this work, two mechanisms were examined in which the phenol reactant adsorbs through the oxygen functional group (vertical): the dehydroxylation and tautomerization and dehydroxylation mechanisms. As for the reaction classifications, the transhydrogenation and deoxygenation, dehydroxylation and transhydrogenation, and hydrogen-assisted dehydroxylation mechanisms all represent variations on the hydrogenation reaction mechanism. This is due to the addition of hydrogen to either the oxygen bonded ring carbon in the adsorbed phenol or an adjacent ring carbon, which results in the shift of the oxygen bonded carbon's electronic structure from $C(sp^2)$ to $C(sp^3)$. The direct deoxygenation mechanism will be studied via the dehydroxylation mechanism that accounts for the straight cleavage of the C−O bond. Finally, the tautomerization and dehydroxylation reaction was chosen to act as a model for the tautomerization mechanism.

Until now, the theoretical work on the HDO of phenolic compounds has been limited to some adsorption studies, with a few studies examining the catalytic reaction mechanisms of these compounds. The adsorption of phenol on Ni,[18] Pt,[19] Rh,[19] Pd,[20,21] and Fe[21] monometallic surfaces has been studied, and they have shown that the horizontal adsorption of phenol results in chemisorption, which significantly distorts the molecule's bonds, whereas the vertical adsorption of phenol on the surface occurs through the oxygen function group with a weak adsorption strength and minimal molecular distortion. Wang et al.[22] studied a single deoxygenation reaction mechanism for the conversion of phenol to a pure carbon chain on the Ni(111) surface and showed that the rate limiting step was likely to be the cleavage of the C−O bond and that the reaction was highly endothermic on the Ni(111) surface. In addition, the cleavage of the O−H bond in phenol adsorbed on Pt and Rh surfaces has been studied.[19]

In addition to this work on monometallic surfaces, the adsorption of numerous phenolic compounds has also been studied on bimetallic and CoMo or Mo sulfide catalyst surfaces.[7,15,23,24] The horizontal adsorption of the phenolic compounds has been shown to be significantly weakened on bimetallic NiFe[15] or PdFe[23,25] surfaces, which suggests a possible switch in the adsorption configuration to vertical adsorption through the oxygen functional groups. This vertical adsorption through the oxygen functional groups is similar to the results seen for phenolic adsorption on the CoMo or Mo sulfide surfaces.[7,24] Finally, Badawi et al.[7] studied a single direct deoxygenation and hydrogenation reaction mechanism on CoMo and Mo sulfide surfaces and found that the addition

dx.doi.org/10.1021/cs501403w | ACS Catal. 2015, 5, 523−536

of the Co into the Mo sulfide surface promoted the direct deoxygenation mechanism significantly more than the hydrogenation mechanism.

To better understand and control the catalyzed HDO reaction of phenolic compounds, a detailed examination of the several possible deoxygenation mechanisms is necessary. From our previous work on a PdFe bimetallic catalyst surface, we identified the Fe surface as the likely HDO catalytically active surface,[23,25] and the Pd likely provides an H_2 activation site as well as stabilizing the metallic Fe surface and preventing catalyst deactivation through Fe oxidation.[26,27] Here, we present a detailed study of the minimum energy pathways (MEPs) of five possible deoxygenation mechanisms (Scheme 1) on the Fe(110) and Pd(111) surfaces to verify that the Fe surface is HDO active and the Pd surface is not, as well as to identify the most probable catalytic deoxygenation mechanism for phenol. Because experiments have shown that the Pd/Fe bimetallic surfaces are composed of Fe surfaces with small Pd patches[23,27] and theoretical results have shown that aromatic species preferentially adsorb away from the Pd patches in the Pd/Fe surfaces,[25] the mechanistic conclusions gained in this study on the Fe surface are expected to be extendable to the Pd/Fe system. In addition to the MEP investigations, we evaluate each mechanism presented in Scheme 1 both energetically and kinetically by estimating the rate constants for each mechanism using transition state theory. In this work, phenol acts as a model phenolic compound, and the Fe(110) and Pd(111) model surfaces were chosen because they are the closest packed facets for BCC Fe and FCC Pd metals.[28] Work performed by Wang et al.[29] and Nørskov et al.[30] has shown that the transition state structure for a given reaction mechanism is relatively independent of the metal type and depends more on the metal surface geometry. This suggests that the transition state and reaction intermediate structures identified in this work will be directly applicable to other transition metals with similar crystal facets. Overall, this work provides a significant insight into the reaction mechanisms for the catalytic HDO of phenolic compounds. The details for the theoretical method and calculation details used for this work are provided in section 2. The major results are then presented in section 3. Finally, conclusions are drawn in section 4.

2. METHODS

The theoretical calculations presented in this work were performed using the Vienna Ab Initio Simulation (VASP) package.[31,32] These density functional theory (DFT) calculations were performed using the generalized gradient approximation, which was parametrized with the Perdew–Wang 91 (PW91)[33,34] functional. This method was combined with VASP's projector augmented waves[35,36] to solve the Kohn–Sham equations. The addition of van der Waals corrections was investigated by calculating the reaction energy for the deoxygenation step in the DHOx mechanism (see Scheme 1) with both the PW91 functional and the optB88[37,38] functional, and the reaction energy was found to change by only 0.08 eV. Therefore, the entirety of the work presented here has been performed with the PW91 functional.

The surfaces were modeled using p(4 × 4) supercells to minimize the lateral interactions between the repeating supercells due to VASP's implementation of periodic boundary conditions. The near surface structure was modeled using four metal layers, the bottom two of which were kept fixed during the optimization. The number of metal layers was tested by increasing the substrate to five layers (bottom three fixed) for the deoxygenation step in the DHOx mechanism (see Scheme 1) and was found to change the reaction energy by only 0.003 eV. All other atoms, including the adsorbates atop the metal slab, were allowed to relax to find the optimum structural configuration. In addition to these parameters, the repeating supercells in the $\hat{z}$ direction were separated by either ∼13 or 18 Å of vacuum when studying either the horizontal or vertical adsorption of phenol, respectively. The bulk FCC Pd and BCC Fe unit cells were optimized, and the calculated lattice constants were found to be 3.957 and 2.827 Å, respectively. These results agree well with previous work.[39−41]

These model supercells were sampled using a (3 × 3 × 1) Monkhorst–Pack[42] mesh, and the kinetic energy cutoff for the plane wave basis set was set at 400 eV. The Methfessel–Paxton[43] ($N = 1$) smearing method was used with a smearing width of 0.1 eV to improve convergence, and the total energy was extrapolated to 0 K. Because Fe is known to be ferromagnetic and O is a spin-polarized atom, spin-polarization effects were accounted for in all calculations; also, the effect of dipole interactions between the consecutive supercells was considered to be significant and dipole corrections were imposed in $\hat{z}$ for each calculation performed.[44] The total energy was converged to at least 10^{-4} eV for all systems, and the systems were considered to be fully optimized when the forces between atoms were <0.03 eV/Å.

The MEP for each reaction was investigated using first the nudged elastic band (NEB)[45,46] method, followed by the climbing image nudged elastic band (CINEB)[47] method to determine the transition state structure. First, the stable minimum energy configurations were identified for both the reactants and products for a given elementary reaction. We then linearly interpolated between these configurations to introduce a number of "images" along the MEP. By using the NEB and CINEB methods consecutively, we were able to identify the transition state structures and activation energy barriers for each elementary reaction studied. The CINEB calculated energies were then plotted along a reaction coordinate defined as the mean squared displacement of all of the atoms in the model systems. If a given reaction mechanism had an intermediate minimum present, the nearest image was fully relaxed to determine if the minimum was a true minimum. If the minimum was a true minimum, the reaction mechanism was then separated into two mechanisms that were then investigated using the NEB and CINEB methods. Finally, the transition state structures were confirmed by calculating their vibrational frequencies and determining that only a single, unique imaginary normal mode eigenvector was present.[48] The presence of this eigenvector then confirms that the transition state was at a first order saddle point. If more than one unique normal mode eigenvector is present, the transition state was further investigated by employing the dimer method.[49] All vibrational frequencies were calculated by allowing the entirety of the adsorbed or coadsorbed species and all surface metal atoms in contact with the adsorbed species to fully relax while all other atoms in the model systems were kept fixed.

All reaction mechanisms were analyzed using the reaction energy (eq 1) and the activation energy (eq 2) as defined as

$$E_{rxn} = E_{products} - E_{reactants} \quad (1)$$

$$E_{act} = E_{transition\ state} - E_{reactants} \quad (2)$$

dx.doi.org/10.1021/cs501403w | ACS Catal. 2015, 5, 523−536

where $E_{\text{transition state}}$, $E_{\text{reactants}}$, and E_{products} are the total energies of the transition state, reactant, and product configurations. The energy shown in the MEP figures for all reactions is the adsorption energy which was defined by

$$E_{\text{ads}} = E_{\text{adsorbates+surface}} - E_{\text{surface}} - \sum_{\text{adsorbates}} E_{\text{gas phase molecule}} \quad (3)$$

where $E_{\text{adsorbates+surface}}$, E_{surface}, and $E_{\text{gas phase molecule}}$ are the total energies of the adsorbed surface system, the clean surface, and the gas phase adsorbates for the given system. For the MEP energies, the adsorption energies of the various structures were relative to gas phase phenol and a hydrogen molecule when necessary. The notation used to describe the adsorbates' positions on the metal surfaces is consistent with our previous work.[21,25]

In addition to the energetic analysis and MEP investigations, we calculated the zero-point energy (ZPE) corrections for the activation and reaction energies and estimated the forward rate constant and equilibrium constant using transition state theory. The forward reaction rate constant was calculated according to[50]

$$k_f = \left(\frac{k_B T}{h}\right)\left(\frac{q^{\ddagger}}{q}\right) e^{-E^0_{\text{act,f}}/k_B T} \quad (4)$$

where k_B and h are Boltzmann's and Planck's constants, respectively; $E^0_{\text{act,f}}$ is the ZPE corrected activation energy for the forward reaction, T is the temperature in Kelvin, and q and $q^{\ddagger}$ are the vibrational partition functions for the initial and transition state structures. The vibrational partition functions were calculated according to

$$q = \Pi_i \frac{1}{1 - e^{-h\nu_i/k_B T}} \quad (5)$$

where ν_i are the vibrational frequencies calculated using DFT for the initial, transition, and final state structures for each elementary reaction found during the MEP investigations. This derivation of the vibrational partition function sets the ZPE for the vibrational frequencies to zero. Using similar equations, merely reversed, the rate constant for the reverse reaction (k_r) for each of the elementary steps found during the MEP investigations were calculated. The equilibrium constant was then calculated using the forward and reverse rate constants calculated according to

$$K_{eq} = \frac{k_f}{k_r} \quad (6)$$

3. RESULTS AND DISCUSSION

The stable initial and final structures for the MEP studies presented here were investigated in our previous work for the adsorption of phenol on the Pd(111) and Fe(110) surfaces[21] and benzene adsorbed on the Fe(110) surface.[25] Benzene's adsorption on the Pd(111) surface has been well characterized by Morin et al.[51] and Liu et al.[52] Additional adsorption and coadsorption studies needed to calculate the MEP for each reaction presented in Scheme 1 were performed in the form of the adsorption of phenyl, coadsorption of benzene and oxygen or hydroxyl, and coadsorption of phenol and hydrogen. In addition, the diffusion of hydrogen on the Fe(110) surface around the coadsorbed phenol was studied and the diffusion barriers were found to be small in the presence of phenol and did not significantly differ from the diffusion of hydrogen across the clean Fe(110) surface. These results are presented in detail in the Supporting Information, but they have no significant impact on the following investigation of the mechanisms of phenol's deoxygenation.

3.1. Overview of the Phenol Deoxygenation Reactions on Fe(110) and Pd(111). To determine each surface's effectiveness at assisting with the reactions presented in Scheme 1, we first calculated the reaction energies for the elementary deoxygenation step for each reaction, except for the tautomerization and dehydroxylation (Taut. and DHOx) mechanisms, which show the elementary tautomerization reaction steps. The resulting structures and reaction energies are shown in Figures 1 and 2.

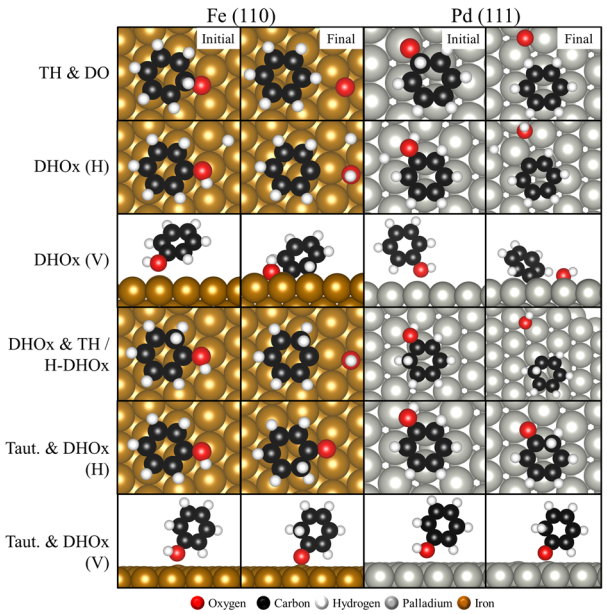

Figure 1. Elementary deoxygenation reaction steps for the TH and DO, DHOx, DHOx and TH, and H-DHOx reactions along with the elementary tautomerization reaction steps for the Taut. and DHOx reaction presented in Scheme 1 on Fe(110) and Pd(111).

From these results, it is clear that the majority of the deoxygenation reactions on the Pd(111) surface are highly endothermic, requiring a reaction energy anywhere from ~0.5 to 1.6 eV to transfer from the reactants to the deoxygenated products. The only exception to this trend was found for the TH and DO reaction, for which the reaction energy was exothermic. On the Fe(110) surface, almost all of the deoxygenation reactions are exothermic, with reaction energies ranging from ~-0.4 to −1.1 eV. Only the Taut. and DHOx (V) reaction on the Fe(110) surface is not exothermic with a significantly endothermic reaction energy. Work performed by Wang et al.[29] has shown that there is a strong BEP relationship between the reaction energy and the activation energy barrier for numerous reactions based on the structural similarity between the transition state and final state.[30] These relations, along with our results in Figure 2, suggest that the deoxygenation reactions are not likely to occur on the Pd(111) surface at reasonable operating temperatures because of the highly endothermic nature of these key reaction steps and the probability of significantly large activation energies. The

dx.doi.org/10.1021/cs501403w | ACS Catal. 2015, 5, 523−536

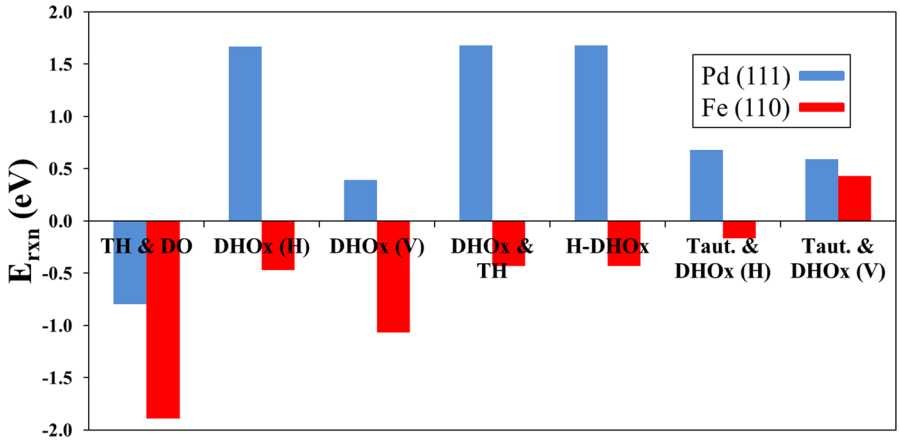

Figure 2. Reaction energies for the elementary deoxygenation reaction steps for the TH and DO, DHOx, DHOx and TH, and H-DHOx reactions along with the elementary tautomerization reaction steps for the Taut. and DHOx reaction presented in Figure 1.

only exception to this trend was the TH and DO reaction on the Pd(111) surface. Therefore, our detailed investigations into the deoxygenation reaction mechanisms, intermediates, and transition states will focus on the Fe(110) surface with the inclusion of the TH and DO reaction on Pd(111) because, on the basis of the exothermic nature of the elementary deoxygenation reaction energies, these reactions have a higher probability of producing the deoxygenated products.

3.2. Phenol Deoxygenation MEP Results. *3.2.1. Trans-hydrogenation and Deoxygenation (TH and DO) Mechanism.* The first mechanism examined here is the trans-hydrogenation and deoxygenation (TH and DO) mechanism, shown in Scheme 1. In this reaction, the OH functional group will rotate about the C−O bond and the OH bond will break as the H from that group bonds with the ring carbon bonded to the oxygen. The oxygen then dissociates from the aromatic ring, leaving benzene and oxygen coadsorbed on the surface. This mechanism was first presented by Orita et al.,[20] who studied the formation of phenol from benzene and oxygen on the Pd(111) and (100) surfaces. This preliminary study investigated the energetic stability of the initial, final, and major intermediate configurations without delving into the MEP and finding the activation energy barriers and transition state structures for this reaction. Here, we present a detailed investigation into the MEP, transition states, and activation energy barriers for the TH and DO reaction on both the Fe(110) and Pd(111) surfaces.

The resulting TH and DO MEP on the Fe(110) surface is shown in Figure 3. This mechanism first proceeds through a complete 180° rotation of the OH group around the C−O bond with a small activation energy barrier of 0.21 eV and a reaction energy of 0.03 eV. Next, the OH group partially rotates about the C−O bond, followed by the breaking of the O−H bond and the formation of the C−H bond. This step has a large activation energy barrier of 2.03 eV and is a nearly energy-neutral reaction with a reaction energy of 0.04 eV. Finally, the C−O bond is broken, and the resulting benzene and oxygen relax away from each other into the 3-fold 30° and 3-fold adsorption sites, respectively, with an activation energy barrier of 0.15 eV and a reaction energy of −1.89 eV. Overall, the second step in the TH and DO reaction on the Fe(110) surface is the limiting reaction step with an activation energy barrier that is an order of magnitude larger than the next largest barrier. In addition, the first two reaction steps are nearly

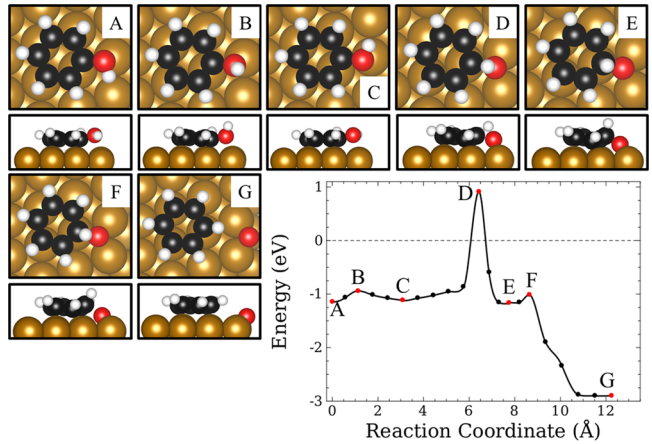

Figure 3. Reaction mechanism MEP for the TH and DO of phenol on the Fe(110) surface. Sphere coloring is identical to that shown in Figure 1, and the energy shown in the MEP is the adsorption energy of the system relative to gas phase phenol.

energy-neutral (meaning that there is no significant energy gain or loss between the products and reactants), whereas the last reaction step is significantly exothermic. The overall reaction energy for the TH and DO reaction on the Fe(110) surface shows the reaction to be highly exothermic.

The TH and DO mechanism on Pd(111) (Figure 4) proceeds in a manner similar to that seen on Fe(110) (Figure 3). First, the OH group rotates around the C−O bond by 180° with a small activation energy barrier of 0.34 eV and a reaction energy of 0.001 eV. Second, the O−H bond is broken and the C−H bond is formed, which has an activation energy barrier of 2.63 eV and an endothermic reaction energy of 1.32 eV. Third, the C−O bond breaks, and the coadsorbed benzene and oxygen relax into the bridge 30° and hcp adsorption sites, respectively. This step has an activation energy barrier of 0.72 eV and a reaction energy of −0.80 eV. Finally, the coadsorbed oxygen diffuses across the surface into an adjacent fcc site with an energy barrier of 0.33 eV and a reaction energy of −0.25 eV. Overall, the second step in the TH and DO reaction on the Pd(111) surface is the limiting reaction step, similar to the Fe(110) surface; however, unlike the Fe(110) surface, this reaction on the Pd(111) surface has two major activation energy barriers: the breaking of the O−H bond combined with the formation of the C−H bond (second peak) and the

dx.doi.org/10.1021/cs501403w | ACS Catal. 2015, 5, 523−536

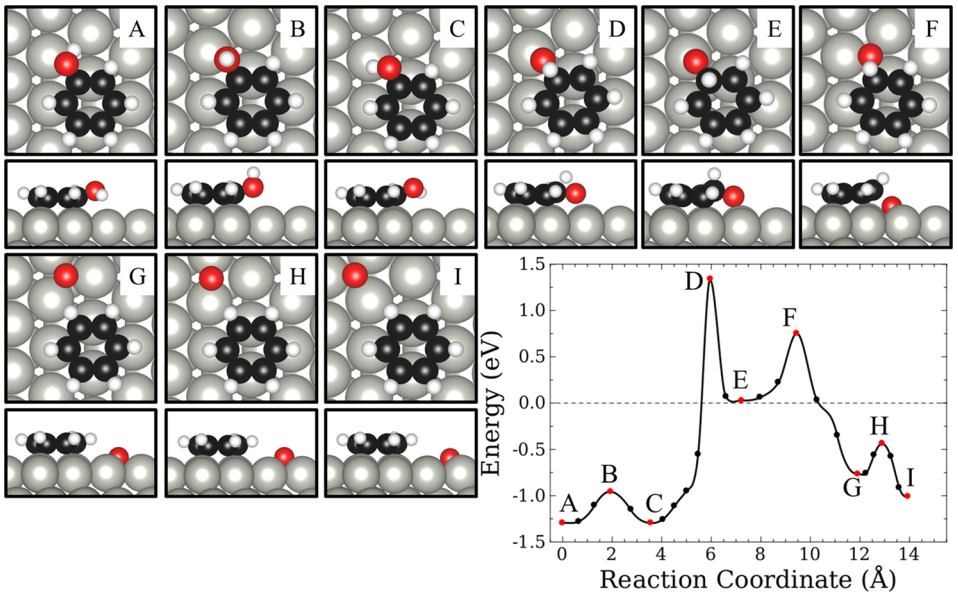

Figure 4. Reaction mechanism MEP for the TH and DO of phenol on the Pd(111) surface. Sphere coloring is identical to that shown in Figure 1, and the energy shown in the MEP is the adsorption energy of the system relative to gas phase phenol.

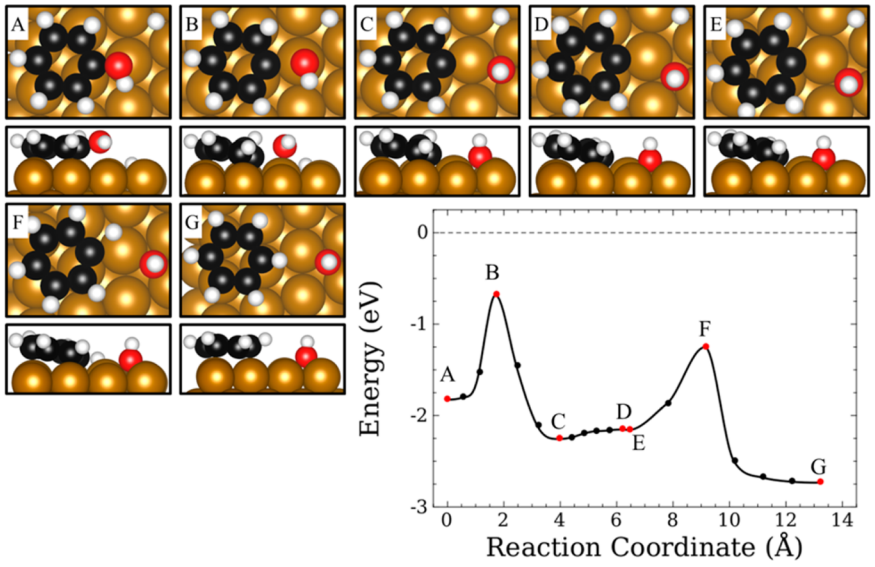

Figure 5. Reaction mechanism MEP for the DHOx (H) reaction for phenol on the Fe(110) surface. Sphere coloring is identical to that shown in Figure 1, and the energy shown in the MEP is the adsorption energy of the system relative to gas phase phenol and half an H_2 molecule.

breaking of the C−O bond (third peak). In addition, the reaction energy results show that the first reaction step is nearly energy-neutral, the second step is highly endothermic, and the last two steps are exothermic; together these energies show that the overall reaction energy is slightly endothermic.

A comparison between the TH and DO reaction mechanism on the Fe(110) and Pd(111) surfaces shows several significant differences. First, the activation energy barrier for the limiting reaction step is ∼0.6 eV smaller on the Fe(110) surface over the Pd(111) surface. Second, the overall reaction energy for the TH and DO reaction on the Fe(110) surface is highly exothermic, whereas the reaction on the Pd(111) surface is endothermic. Third, the activation energy and reaction energy for the elementary step resulting in the cleavage of the C−O bond is ∼0.6 eV and ∼1.0 eV larger, respectively, on the Pd(111) surface relative to the Fe(110) surface. However, an examination of the transition state and reaction intermediate structures for each peak on the Fe(110) and Pd(111) surfaces shows that although the activation energy barriers and reaction energies are significantly different between the two surfaces, the molecular structures are nearly identical. This agrees with the work performed on simpler molecules by Wang et al.[29] and supports the theory that the transition state structure is independent of metal type.[30] Overall, these results suggest that the Pd(111) surface is not active for the deoxygenation of phenol. Therefore, all further MEP investigations will be performed solely on the Fe(110) surface.

3.2.2. Dehydroxylation (DHOx) Mechanism. The second mechanism examined here is the dehydroxylation (DHOx) mechanism, shown in Scheme 1. In this reaction, we start with phenol and hydrogen coadsorbed on the Fe(110) surface. Next, the C−O bond is broken, which leaves a surface with a phenyl

dx.doi.org/10.1021/cs501403w | ACS Catal. 2015, 5, 523−536

species (C_6H_5), hydroxyl, and hydrogen all coadsorbed. Finally, the surface hydrogen binds at the empty site on the phenyl species to form benzene and hydroxyl coadsorbed on the surface. The resulting MEP and major structures for horizontally adsorbed phenol for this mechanism (labeled DHOx (H)) on the Fe(110) surface are shown in Figure 5.

The activation energies for the B, D, and F transition states were found to be 1.14, 0.103, and 0.91 eV, respectively. For each of the elementary reaction steps (A to C, C to E, and E to G), the reaction energies were calculated to be −0.43, 0.10, and −0.58 eV. These results show that two elementary reaction steps compete for the limiting reaction step, the breakage of the C−O bond and the formation of the C−H bond steps, and both of these reactions are exothermic. Overall, this mechanism is highly exothermic, with a reaction energy of −0.9 eV, and the largest activation energy barrier is ∼0.9 eV smaller than that found for the TH and DO mechanism on Fe(110). Therefore, the DHOx reaction mechanism is significantly more likely to act as the mechanism by which phenol is converted to benzene as compared with the TH and DO mechanism. In addition, comparing the results for the elementary dehydroxylation step (peak A to C) between Fe(110) and Ni(111),[22] it is clear that the deoxygenation reaction is facilitated significantly more by the Fe(110) surface. This is seen in the ∼0.5 eV decrease in activation energy and ∼1.2 eV decrease in the reaction energy, switching the reaction from endothermic to exothermic, relative to this reaction on the Ni(111) surface.[22]

From the preceding reaction (Figure 5), the second peak results in an odd rearrangement of the surface species in which the phenyl ring rotates on the surface and the OH group shifts into an adjacent 3-fold site (structures C−E in Figure 5). Because the surface hydrogen in the reaction is closer to the coadsorbed OH group relative to the coadsorbed phenyl species, we have investigated the possibility that this surface rearrangement of the coadsorbed species is due to a competing mechanism involving the formation of water over benzene. This competing mechanism is shown in Figure 6 and involves the surface diffusion of the OH species to atop an Fe atom and then binding with the surface hydrogen species to form water on the top site, which has been shown to be the most favorable adsorption site for water on the Fe(110) surface.[28]

The MEP results for this side reaction for the formation of water show that the reaction is split into two peaks. The first peak involves the surface diffusion of the OH group to the short bridge site and has an activation energy of 0.11 eV and a reaction energy of 0.07 eV. The second peak is caused by the bonding of the surface OH and H species to form water on the top site and has an activation energy of 1.41 eV and a reaction energy of 0.85 eV. When compared with the DHOx reaction mechanism results (Figure 5), it is clear that the formation of benzene is more energetically feasible than the formation of water. The possibility that water could form immediately upon the cleavage of the C−O bond, without the OH adsorption intermediate step (A−C in Figure 8), was also investigated by moving the OH group to a 3-fold site directly adjacent to the 3-fold site with the surface H (Supporting Information Figure S6). However, upon structural optimization, the OH and H surface species diffused away from each other instead of combining to form water. On the basis of these results, water formation on the Fe(110) surface is not likely to significantly impede the production of benzene by reacting with surface hydrogen before benzene can be formed, but the continued presence of oxygen species on the Fe surface likely impedes

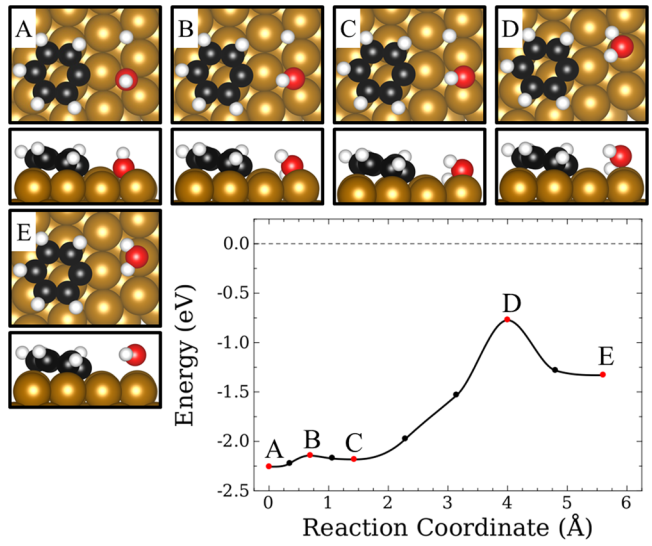

Figure 6. Reaction mechanism MEP for the side reaction from the DHOx (H) reaction for the formation of water from the hydrogen and hydroxyl species coadsorbed with horizontal phenyl on the Fe(110) surface. Sphere coloring is identical to that shown in Figure 1, and the energy shown in the MEP is the adsorption energy of the system relative to gas phase phenol and half an H_2 molecule.

benzene formation by blocking the adsorption of phenol. The highly endothermic nature of the water formation reaction on Fe(110) coadsorbed with phenyl (Figure 6) is consistent with previous work performed by Wang et al.[29] on both a flat and a stepped Fe surface. The unfavorable nature of the water formation reaction on Fe surfaces suggests that pure Fe catalysts are likely poisoned by surface oxygen under HDO conditions as the surface oxygen will form Fe oxides. In our previous work,[26,27] we have shown that in the bimetallic Pd/Fe system, the Pd likely promotes the formation of water, because Pd has been shown to exothermically form water from surface OH and H[29] and stabilizes the metallic Fe state, which protects the Fe surface from being oxidized and deactivated. Therefore, the addition of dopants to the Fe surface could significantly reduce the energy required to remove surface oxygen species and maintain the active Fe surface during reaction.

In addition to the DHOx mechanism proceeding from the horizontally adsorbed phenol, we examined the DHOx mechanism with phenol starting in a vertical adsorption configuration (labeled DHOx (V)). For this mechanism, we started with phenol adsorbed on the Fe(110) surface through the hydroxyl group. Next, the C−O bond is broken, which leaves a surface with a vertical phenyl species (C_6H_5) and hydroxyl group coadsorbed. Finally, a surface hydrogen would then bind to the empty site on the phenyl species to form benzene, which has desorbed from the surface, and hydroxyl, which remains adsorbed on the surface. However, during the optimization of the system, the horizontal adsorption of phenol through the aromatic ring occurred before the C−O bond broke. The resulting MEP and major structures for this reaction on the Fe(110) surface are shown in Figure 7.

The MEP result for this reaction for the DHOx (V) mechanism shows that the reaction is split into two peaks. The first peak involves the rotation of the aromatic ring in the gas phase with the phenol remaining bound to the surface through the hydroxyl group with an activation energy of 0.08 eV and a reaction energy of −0.02 eV. The second peak is caused by the

dx.doi.org/10.1021/cs501403w | ACS Catal. 2015, 5, 523−536

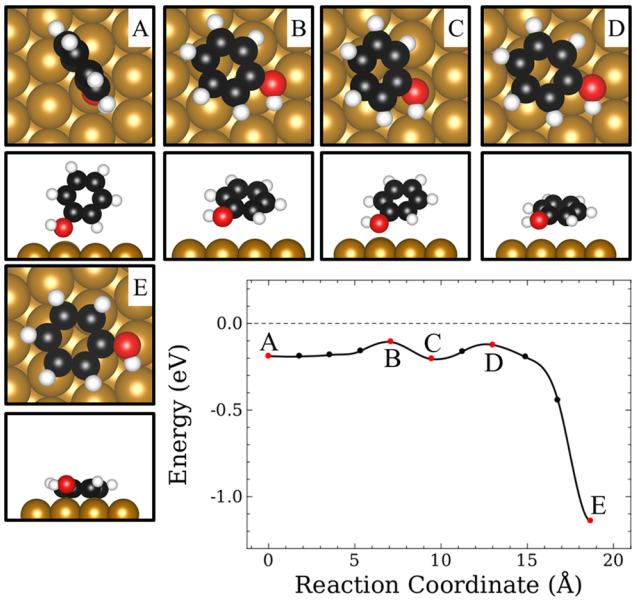

Figure 7. Reaction mechanism MEP for the DHOx (V) reaction for phenol on the Fe(110) surface. Sphere coloring is identical to that shown in Figure 1, and the energy shown in the MEP is the adsorption energy of the system relative to gas phase phenol.

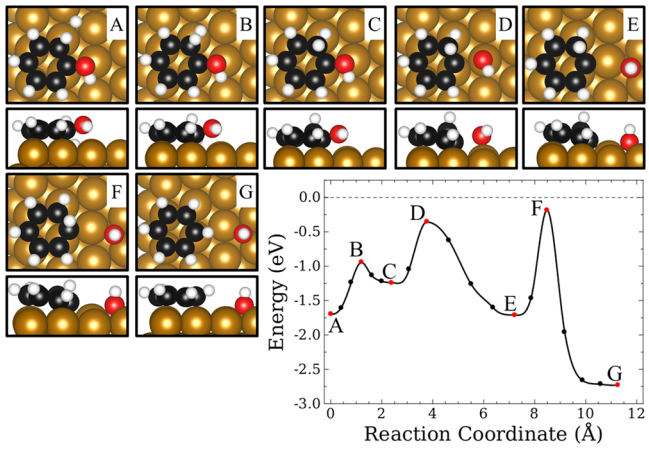

Figure 8. Reaction mechanism MEP for the DHOx and TH reaction of phenol on the Fe(110) surface. Sphere coloring is identical to that shown in Figure 1, and the energy shown in the MEP is the adsorption energy of the system relative to gas phase phenol and half an H_2 molecule.

tilting of the aromatic ring toward the surface for adsorption. This step involves the breaking of the weak O−M bond with an activation energy and overall reaction energy of 0.08 eV and −0.94 eV, respectively. From these results, the DHOx (V) for phenol will not occur on the Fe(110) surface before the C−O bond can be broken, so the phenol will instead horizontally adsorb to make the C−O break more favorable.

3.2.3. Dehydroxylation and Transhydrogenation (DHOx and TH) Mechanism. The third mechanism examined here is the dehydroxylation and transhydrogenation (DHOx and TH) mechanism, shown in Scheme 1. In this reaction, we start with phenol and hydrogen coadsorbed on the Fe(110) surface. Next, the surface hydrogen then bonds to a carbon adjacent to the C−O bond, partially hydrogenating the aromatic ring. The C−O bond then breaks, leading to the coadsorption of OH and a partially hydrogenated phenyl species on the Fe(110) surface. Finally, the additional hydrogen on the aromatic ring shifts and bonds with the dehydroxylated carbon, resulting in the formation of benzene coadsorbed with a hydroxyl group on the Fe(110) surface. The resulting MEP and the major atomic configurations for this reaction are shown in Figure 8.

The calculated activation energies for the B, D, and F transition states were found to be 0.76, 0.88, and 1.53 eV, respectively. For each of the elementary reaction steps (A to C, C to E, and E to G), the reaction energies were calculated to be 0.46, −0.47, and −1.02 eV.

Each elementary step in this reaction has a sizable activation energy barrier, with the limiting reaction step occurring in the third step, where the added ring hydrogen shifts its bonding between the ring carbons to form benzene (configurations E to G in Figure 8). This elementary step has an activation energy barrier that is 0.65 eV larger than the next-highest barrier. The reaction energy results are exothermic for all elementary steps, except for the partial hydrogenation of the phenol adsorbate, which is an endothermic reaction. Overall, this reaction is highly exothermic. Compared with the TH and DO mechanism on Fe(110), the DHOx and TH mechanism is significantly more favorable, with the activation energy barrier for the limiting reaction step for the DHOx and TH mechanism being 0.5 eV smaller than the limiting reaction step on the TH and DO mechanism. The comparison with the previous mechanisms shows that the DHOx (H) mechanism is more energetically favorable than the DHOx and TH mechanism, as seen in the ∼0.4 eV decrease in the limiting reaction step's activation energy barrier.

The energetic comparison of the DHOx and TH mechanism with the horizontal DHOx mechanism provides some interesting insights into the phenol surface reactions on Fe(110). First, the activation energy barrier to the hydrogenation of phenol on this surface appears to be ∼0.7 eV, with a reaction energy of ∼0.5 eV. This energy barrier is ∼0.4 eV smaller than the limiting reaction step's energy barrier for the DHOx reaction, which suggests that the hydrogenation of phenol is energetically possible on the Fe(110) surface. Furthermore, the partial hydrogenation of the phenol adsorbate decreases the energy required to break the C−O bond by ∼0.3 eV. This latter result suggests that partially hydrogenating the phenol adsorbate assists in the deoxygenation reaction; however, the transhydrogenation step has a large reaction barrier. Overall, these results show that the DHOx and TH mechanism is moderately energetically favorable; however, the DHOx mechanism is still the more probable deoxygenation reaction mechanism for the conversion of phenol to benzene.

3.2.4. Hydrogen Assisted Dehydroxylation (H-DHOx) Mechanism. The fourth mechanism examined here is the hydrogen assisted dehydroxylation (H-DHOx) mechanism, shown in Scheme 1. In this reaction, a surface hydrogen atom bonds to a ring carbon adjacent to the C−O bond in the coadsorbed phenol molecule, partially hydrogenating the aromatic ring. The C−O bond is then broken, and a second surface hydrogen atom then binds to the empty carbon site on the aromatic molecule. Finally, the additional hydrogen on the aromatic ring then dissociates from the ring, which forms benzene, hydrogen, and hydroxyl coadsorbed on the Fe(110) surface. The assistance of a spectator hydrogen has been studied for several other reactions and has been shown to significantly reduce the energy barriers for C−O bond cleavage in the catalytic conversion of CO_2 on Ni,[53] the desorption

dx.doi.org/10.1021/cs501403w | ACS Catal. 2015, 5, 523−536

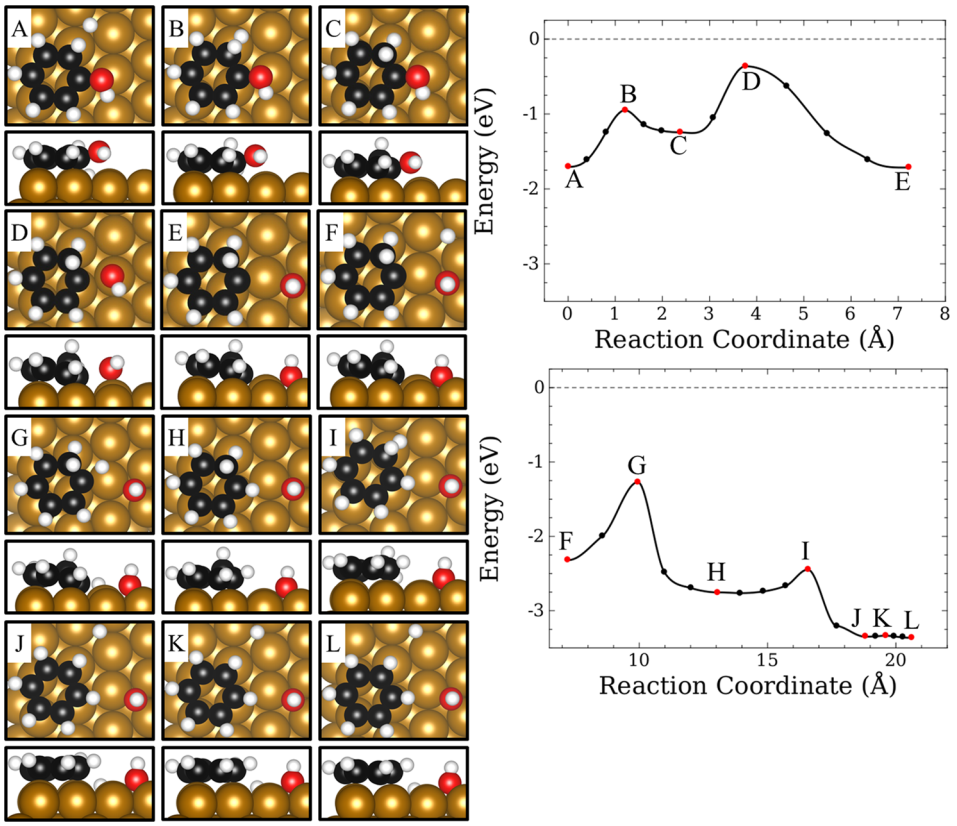

Figure 9. Reaction mechanism MEP for the H-DHOx reaction of phenol on the Fe(110) surface. Sphere coloring is identical to that shown in Figure 1. The MEP was split into two graphs because the adsorption of a second hydrogen on the surface is necessary at step F for the reaction to continue. Because of the second hydrogen added at step F, the energy shown in the MEP is the adsorption energy of the system relative to gas phase phenol and either half an H_2 molecule for the path A-E or a whole H_2 molecule for the path F-L.

energy of NO_3 on Ag doped Al_2O_3,[54] and CO dissociation on Fe.[55] The resulting MEP and the major atomic configurations for this reaction are shown in Figure 9.

This reaction mechanism has the largest number of elementary steps of all the reactions previously examined, with the transition states (images B, D, G, I, and K) having activation energy barriers of 0.76, 0.88, 1.05, 0.31, and 0.01 eV, respectively. The largest barrier to this reaction occurs at the third step, which involved the formation of the C−H bond at the empty carbon site. However, this barrier is only ∼0.2 eV larger than the C−O bond cleavage energy barrier. The reaction energy results for each elementary step were found to be 0.46, −0.47, −0.44, −0.59, and −0.02 eV for the A to C, C to E, F to H, H to J, and J to L elementary reaction steps, respectively. These results show that all of the reaction steps are exothermic, except for the first elementary step, which is the partial hydrogenation of the phenolic ring. The overall reaction energy is ∼-1 eV, and the reaction is highly exothermic. A comparison of the results obtained here with the previous reaction mechanisms shows that this mechanism has an energetic favorability similar to that seen for the DHOx (H) mechanism. This suggests that the partial hydrogenation mechanism for HDO likely competes, energetically, with the direct deoxygenation mechanism on the Fe(110) surface.

3.2.5. Tautomerization and Dehydroxylation (Taut. and DHOx) Mechanism. The fifth, and final, mechanism examined here is the tautomerization and dehydroxylation (Taut. and DHOx) mechanism, shown in Scheme 1. In this reaction, phenol undergoes tautomerization to cyclohexadienone, which is then subsequently hydrogenated. The C−O bond is then cleaved and followed by the formation of benzene. This mechanism was studied with the phenol adsorbed both horizontally (Figure 10) and vertically (Figure 11) on the Fe(110) surface. These mechanisms have been labeled as Taut. and DHOx (H) and Taut. and DHOx (V) for the horizontal and vertical mechanisms, respectively.

From the energy barrier for the tautomerization reaction in both configurations, it is clear that this reaction mechanism is significantly less favorable than the majority of the paths previously examined. Therefore, we studied only the elementary tautomerization MEP and did not fully examine the entire MEP for this reaction's conversion of phenol to benzene.

The resulting energy barriers for the Taut. and DHOx reaction shows that this elementary reaction step has activation energies and reaction energies of 2.03 eV and −0.17 eV for the horizontal mechanism and 2.41 and 0.43 eV for the vertical mechanism, respectively. These barriers are significantly higher than those found for the DHOx, DHOx and TH, and H-DHOx mechanisms, and the vertical tautomerization reaction barrier is even higher than that found for the TH and DO mechanism on the Fe(110) surface. The comparison between the horizontal and vertical Taut. and DHOx reaction mechanisms show that the greater interaction between the adsorbate and surface, as seen in the horizontal mechanism, decreases the energy barrier to the tautomerization reaction by ∼0.4 eV and the cyclohexadienone intermediate species is significantly stabilized by the greater surface interaction relative to the vertical adsorption mechanism. These results are similar to those of

dx.doi.org/10.1021/cs501403w | ACS Catal. 2015, 5, 523−536

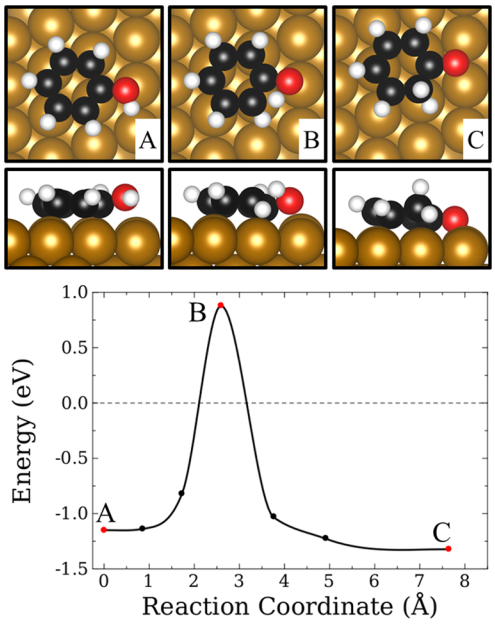

Figure 10. Reaction mechanism MEP for the Taut. and DHOx (H) reaction of phenol on the Fe(110) surface. Sphere coloring is identical to that shown in Figure 1, and the energy shown in the MEP is the adsorption energy of the system relative to gas phase phenol.

Yoon et al.[56] who studied the hydrogenation of phenol on the Pt (111) and Ni(111) surfaces in the absence and presence of water. Under ultrahigh vacuum, the hydrogenation mechanisms that involved the tautomerization of the phenol adsorbate had energy barriers of ∼1.9 eV and ∼1.1 eV on Pt (111) and Ni(111), respectively, which is similar to the Taut. and DHOx barrier presented above. However, with water present in the system, the tautomerization barrier was seen to decrease to ∼0.6 eV as the water molecules facilitated the transfer of a hydrogen atom from the hydroxyl group to the adjacent ortho position on the aromatic ring through the formation and decomposition of hydronium ions. These results show that further study is needed in this area and that the presence of water can greatly affect the reaction mechanisms. Overall, this mechanism is significantly less favorable than the DHOx and H-DHOx mechanisms, under ultrahigh vacuum conditions, which have been identified as the most favorable reaction mechanisms for the deoxygenation of phenol on the Fe(110) surface.

3.3. BEP Relationships. From the results of the preceding MEP investigations, it is clear that the deoxygenation of phenol to benzene has two key steps: the cleavage of the C−O bond and the subsequent formation of the C−H bond. In all of the mechanisms studied, these two steps have the largest energy barriers, which will significantly impede the reaction. Because the cleavage of the C−O bond and the formation of the C−H bond appear to be the key factors governing the catalytic deoxygenation of phenol to benzene, we present two Brønsted−Evans−Polanyi (BEP)[57,58] relationships for these elementary steps in Figure 12. The results for the TH and DO mechanism on the Pd(111) surface fit well with the other data on the Fe(110) surface. This agreement between the BEP results on different surfaces is consistent work by Wang et al.[29] and suggests that even in this more complex reaction, the

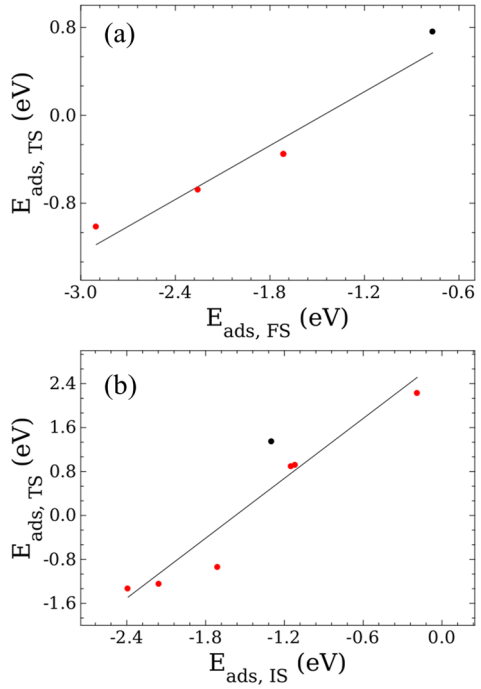

Figure 12. BEP relationships for the elementary C−O cleavage steps (a) and the C−H formation steps (b). The single Pd point (black circle) refers to the results for the TH and DO mechanism on the Pd(111) surface. $E_{ads,\ FS}$, $E_{ads,\ IS}$, and $E_{ads,\ TS}$ are the adsorption energies of the final, initial, and transition states, respectively, relative to gas phase phenol and hydrogen where appropriate via eq 3.

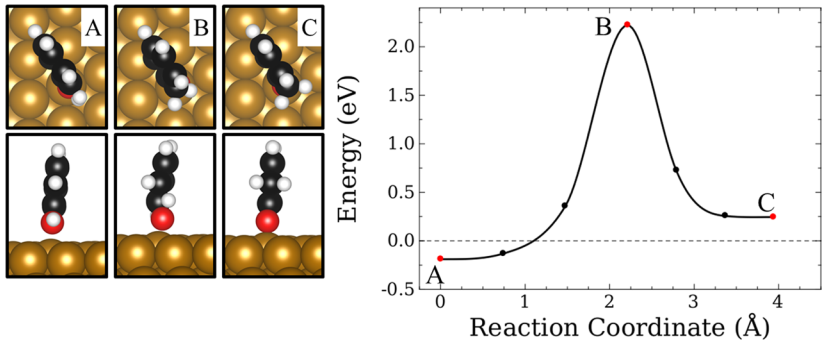

Figure 11. Reaction mechanism MEP for the Taut. and DHOx (V) reaction of phenol on the Fe(110) surface. Sphere coloring is identical to that shown in Figure 1, and the energy shown in the MEP is the adsorption energy of the system relative to gas phase phenol.

dx.doi.org/10.1021/cs501403w | ACS Catal. 2015, 5, 523−536

Table 1. ZPE-Corrected Activation (E^0_{act}) and Reaction Energies (E^0_{rxn}), along with Forward Rate Constants (k_f) and Equilibrium Constants (K_{eq}) for Each Elementary Step in the Reaction Mechanisms Studied in Section 3.2

			T = 350 °C		T = 450 °C	
reaction	E^o_{act} (eV)	E^o_{rxn} (eV)	k_f (s^{-1})	K_{eq}	k_f (s^{-1})	K_{eq}
TH and DO - Fe						
C−OH rotation	0.18	0.03	5.3×10^{11}	2.6×10^{-1}	1.0×10^{12}	2.9×10^{-1}
C−H formation	1.84	−0.06	1.2×10^{-1}	1.2×10^{1}	1.8×10^{1}	1.2×10^{1}
C−O cleavage	0.12	−1.76	5.1×10^{11}	9.0×10^{12}	7.4×10^{11}	7.8×10^{10}
TH and DO, Pd						
C−OH rotation	0.30	−0.01	5.9×10^{10}	1.7×10^{0}	1.4×10^{11}	1.7×10^{0}
C−H formation	2.44	1.30	3.9×10^{-8}	2.5×10^{-13}	2.1×10^{-5}	5.0×10^{-12}
C−O cleavage	0.69	−0.80	2.2×10^{8}	9.5×10^{4}	1.6×10^{9}	1.1×10^{4}
O diffusion	0.32	−0.23	4.9×10^{11}	1.7×10^{0}	1.5×10^{12}	3.5×10^{3}
DHOx (H)						
C−O cleavage	1.04	−0.48	1.1×10^{4}	4.2×10^{3}	1.8×10^{5}	1.4×10^{3}
ring rotation	0.10	0.09	7.2×10^{11}	6.6×10^{-2}	9.4×10^{11}	7.4×10^{-2}
C−H formation	0.87	−0.43	1.5×10^{5}	4.0×10^{3}	1.4×10^{6}	1.3×10^{3}
DHOx (V)						
ring rotation	0.08	−0.02	6.2×10^{9}	1.2×10^{-1}	5.8×10^{9}	9.7×10^{-2}
ring adsorption	0.06	−1.06	1.9×10^{11}	8.2×10^{3}	2.0×10^{11}	1.4×10^{5}
H_2O formation						
OH diffusion	0.07	0.05	2.3×10^{12}	1.6×10^{0}	2.9×10^{12}	1.9×10^{0}
H_2O formation	1.32	0.97	7.7×10^{1}	3.1×10^{-8}	2.3×10^{3}	3.5×10^{-7}
DHOx and TH						
partial hydrogenation	0.75	0.61	2.3×10^{6}	2.0×10^{-5}	1.7×10^{7}	1.0×10^{-4}
C−O cleavage	0.77	−0.56	1.8×10^{7}	3.2×10^{5}	1.4×10^{8}	8.4×10^{4}
C−H formation	1.41	−1.01	8.6×10^{2}	1.1×10^{8}	4.3×10^{4}	7.3×10^{6}
H-DHOx						
partial hydrogenation	0.75	0.61	2.3×10^{6}	2.0×10^{-5}	1.7×10^{7}	1.0×10^{-4}
C−O cleavage	0.77	−0.56	1.8×10^{7}	3.2×10^{5}	1.4×10^{8}	8.4×10^{4}
C−H formation	1.01	−0.27	2.1×10^{4}	2.1×10^{2}	2.8×10^{5}	9.5×10^{1}
partial dehydrogenation	0.17	−0.72	8.5×10^{11}	2.1×10^{6}	1.5×10^{12}	3.7×10^{5}
ring rotation	−0.008	−0.03	2.5×10^{13}	1.6×10^{0}	2.9×10^{13}	1.5×10^{0}
Taut. and DHOx (H)						
tautomerization	1.83	−0.20	1.74×10^{-3}	2.3×10^{1}	2.0×10^{-1}	1.5×10^{1}
Taut. and DHOx (V)						
tautomerization	2.21	0.38	1.7×10^{-7}	2.0×10^{-4}	4.1×10^{-5}	4.5×10^{-4}

transition state structures are relatively independent of metal type.[30] In the following discussions, $E_{ads,\ FS}$, $E_{ads,\ IS}$, and $E_{ads,\ TS}$ are used to denoted the adsorption energies of the final, initial, and transition states, respectively, relative to gas phase phenol and hydrogen where appropriate via eq 3.

For the C−O cleavage BEP relation, we found a good fit for the data when the adsorption energy of the transition state was plotted versus the adsorption energy of the final state (both adsorption energies were calculated relative to gas phase phenol and hydrogen as appropriate). This BEP relation is $E_{ads,TS} = 0.8171E_{ads,FS} + 1.1954$, which has an R^2 value of 0.94 and a MAE (mean absolute error) of 0.14 eV. It is interesting to note that the linear relation predicted for the C−O cleavage reaction step in phenol is quite similar to the general BEP relation predicted for dehydrogenation reactions of $E_{ads,TS} = (0.86 \pm 0.01)E_{ads,FS} + (1.14 \pm 0.02)$.[29] This relation was found to predict the transition state adsorption energy for the C−O cleavage elementary steps with a MAE of 0.16 eV, which suggests that the BEP relations for simple decomposition reactions can be extended to more complex systems, thus reducing the time and effort required to identify catalytic mechanisms.

For the C−H formation BEP relation, we found the best fit when the adsorption energy of the transition state was plotted versus the adsorption energy of the initial state. This BEP relation is $E_{ads,TS} = 1.8166E_{ads,FS} + 2.8554$ with and R^2 value of 0.89 and a MAE of 0.34 eV, which shows that the C−H formation step has a higher error when using BEP relations than the C−O cleavage step. Although the previous reaction was found to agree well with previous BEP relations for simple reactions, this elementary step shows a significant deviation from the work done by Wang et al.;[29] therefore, even though the decomposition of the C−O bond elementary step was easily described by simpler models, it seems likely that the second key step in the deoxygenation of phenol to benzene has a weaker relation to simpler reaction models as compared to the C−O cleavage step. These relations show that the transition state energies for the C−O cleavage reaction step are better predicted by the final state energies for this elementary reaction step and the C−H formation step's transition state energy is better predicted by the initial state energy for this elementary reaction step. As for a prediction of the structure of the transition state species for these two key steps (C−O cleavage and C−H formation), it is clear that our results closely follow Hammond's postulate.[59] According to Hammond's postulate, transition states will more closely structurally resemble whichever species (initial or final state species) that has the closest energy to that of the transition state. This means that

dx.doi.org/10.1021/cs501403w | ACS Catal. 2015, 5, 523−536

exothermic reactions will have transition states which more closely resemble the structure of the reactants and vice versa for endothermic reactions. We see that this is indeed true for the exothermic C−O cleavage and C−H formation reactions presented in our work.

The usefulness of such BEP relations is in being able to estimate the adsorption energy of the transition state (and hence the activation energy) for additional mechanisms purely on the basis of the initial and final state's adsorption energies. As an example of the usefulness of such BEP relations, we examined the possible hydrogenation of phenol's aromatic ring in the para position and compared the BEP predicted activation energy for this reaction to the activation energy for the addition of the hydrogen to the ortho position examined in the DHOx and TH and H-DHOx mechanisms. The results for this comparison are shown in the Supporting Information and suggest that the hydrogenation of the aromatic ring is significantly unfavorable on the Fe(110) surface. Overall, these relations provide a valuable tool that can be used to quickly evaluate the energetic feasibility of additional deoxygenation mechanisms.

3.4. ZPE Corrections and Kinetic Parameters. Using the calculated activation and reaction energies along with the vibrational frequencies for the initial, transition, and final state structures, the activation and reaction energies obtained from the MEP reported in section 3.2 were corrected for the structures ZPE. These ZPE corrected energies are reported in Table 1. In general, the corrections are quite small with the largest changes occurring in the TH and DO mechanism on both Fe(110) and Pd(111) and both of the Taut. and DHOx mechanisms where the activation energy ZPE corrections were ∼0.2 eV. A comparison of the ZPE-corrected activation energies between the mechanisms show that the DHOx and H-DHOx mechanisms compete as the most energetically favorable mechanism in which both have rate-limiting activation energies of ∼1 eV. The next most favorable mechanisms are the DHOx and TH mechanisms and the H_2O formation side reaction with rate-limiting activation energies of ∼1.3 eV. The remaining mechanisms have activation energies of ∼1.8 eV or higher. The overall reaction energies for all of the mechanisms on Fe(110) show the reactions to be very exothermic, with the deoxygenated products strongly favored over the oxygenated aromatic adsorbate. The only mechanisms that are endothermic are the H_2O formation side reaction on Fe(110) and the TH and DO mechanism on Pd(111).

In addition to the ZPE-corrected activation and reaction energies, the DFT calculated vibrational frequencies for the initial, transition, and final state structures for the detailed mechanisms presented in section 3.2 were used to estimate the forward rate constants and equilibrium constants for these reactions using transition state theory (Table 1).

These constants were estimated at both 350 and 450 °C because these temperatures were shown from experiment to be effective temperatures for the production of deoxygenated aromatic compounds from guaiacol.[23] For the reactions with activation energies of ∼1.8 eV or higher, the rate constants are quite small, with the largest rate constants found for the TH and DO mechanism on Fe(110); however, this rate constant is still 3 orders of magnitude smaller than the next most favorable mechanism, the DHOx and TH mechanism. From the energetic analysis, it was clear that the DHOx and TH and H_2O formation mechanisms likely competed because they had similar activation energies. Comparing the estimated forward rate constants for the rate limiting steps for these mechanisms shows that the DHOx and TH is 1 order of magnitude faster than the H_2O formation reaction; however, although the rate constants for these two reactions are similar, the equilibrium constants show that the H_2O formation mechanism has a significantly faster reverse rate constant than its forward rate constant and the DHOx and TH mechanism's forward rate constant dominates over the reverse rate constant. This shows that the formation of H_2O is unlikely on the Fe(110) surface because both the energetic and kinetic parameters show that the dissociation of H_2O dominates over the formation of H_2O. For the DHOx and TH mechanism, the cleavage of the C−O bond and the formation of benzene is clearly kinetically favored; however, the equilibrium constant for the initial step, which consists of the partial hydrogenation of the aromatic ring prior to the cleavage of the C−O bond, shows that the reverse reaction is significantly more likely to occur. This result is in agreement with that seen in Table 1 for the H-DHOx mechanism, where one can see that the partial hydrogenation of the aromatic ring is very unlikely and that the rate constant for the hydrogenation of the aromatic ring on the Fe(110) surface is 4 orders of magnitude smaller than the reverse, dehydrogenation reaction at 450 °C.

Finally, we compare the estimated kinetic parameters for the two energetically most favorable mechanisms: the DHOx (H) and H-DHOx mechanisms. Examining the C−O cleavage elementary step shows that this key step occurs 3 orders of magnitude faster in the H-DHOx mechanism than in the DHOx (H) mechanism, which shows that the change from $C(sp^2)$ to $C(sp^3)$ prior to C−O cleavage significantly weakens the C−O bond, promoting faster deoxygenation when compared with the direct deoxygenation mechanism. However, as discussed above for the DHOx and TH mechanism, the partial hydrogenation of phenol on the Fe(110) surface is significantly unfavorable with the rate at which the dehydrogenation of the partially hydrogenated intermediate species proceeding at 3 orders of magnitude faster than the subsequent cleavage of the C−O bond. This strong driving force against the hydrogenation of phenol's aromatic ring in the H-DHOx mechanism likely prevents this mechanism from occurring on the Fe(110) surface because the dehydrogenation of the key, hydrogenated phenolic intermediate occurs at a much faster rate than the formation of said intermediate. Therefore, the DHOx (H) mechanism is likely the dominant deoxygenation mechanism on Fe(110) because this mechanism was shown to have a strong driving force, both energetically and kinetically, to the deoxygenated, aromatic products. However, further study is needed in this area as the presence of water in the system could greatly affect the energetics and kinetics of the various mechanisms,[56,60] altering the dominant deoxygenation mechanism.

4. CONCLUSIONS

We presented a study of the deoxygenation mechanism for the conversion of phenol to benzene on Fe(110) and Pd(111) using density functional theory. This study proposed and examined five distinct deoxygenation mechanisms: TH and DO, DHOx, DHOx and TH, H-DHOx, and Taut. and DHOx. The reaction energy for the elementary deoxygenation reaction step for each mechanism studied was calculated on both the Fe(110) and Pd(111) surfaces and the reaction energies were found to be highly endothermic on Pd(111), whereas they were found to be exothermic on Fe(110). On the basis of these

dx.doi.org/10.1021/cs501403w | ACS Catal. 2015, 5, 523−536

results, we performed in-depth MEP investigations and estimated the kinetic parameters, using transition state theory and the DFT calculated vibrational frequencies, for the mechanisms on the Fe(110) surface. From the energetic analyses, two mechanisms were identified as competing for the most favorable mechanism: the DHOx and H-DHOx mechanisms. The second-most-favorable mechanism was determined to be the H-DHOx mechanism. Although the H-DHOx mechanism has the highest rate constant for C−O bond cleavage, the rapid dehydrogenation of the key partially hydrogenated intermediate species on this mechanism, as seen in the equilibrium constant results, significantly limits the rate of this mechanism. Therefore, the most favorable phenol deoxygenation mechanism was the DHOx mechanism because each step in this mechanism is both energetically and kinetically favorable.

■ ASSOCIATED CONTENT

Supporting Information

The following file is available free of charge on the ACS Publications website at DOI: 10.1021/cs501403w.

Details concerning the adsorption and coadsorption studies performed to determine the initial and final structures for the MEP investigations presented in section 3.2; the MEP investigation of the surface diffusion of hydrogen near coadsorbed phenol; an in-depth analysis of the vibrational modes of the initial, transition, and final states for all the MEP investigations presented in this work; and the examination of the hydrogenation phenol in the para position on Fe(110) (PDF)

■ AUTHOR INFORMATION

Corresponding Author

*Phone: 509-335-8580. Fax: 509-335-4806. E-mail: js.mcewen@wsu.edu.

Notes

The authors declare no competing financial interest.

■ ACKNOWLEDGMENTS

This work was supported by institutional funds provided to J.S.M. from the Voiland School of Chemical Engineering and Bioengineering and was partially funded by USDA/NIFA through the Hatch Project No. WNP00807 titled: “Fundamental and Applied Chemical and Biological Catalysts to Minimize Climate Change, Create a Sustainable Energy Future, and Provide a Safer Food Supply”. Our thanks also go to the donors of The American Chemical Society Petroleum Research Fund for in part support of this research. We also thank the support from the US Department of Energy (DOE), Office of Basic Energy Sciences, Division of Chemical Sciences, Geosciences, and Biosciences. We acknowledge computational resources provided by the Center for Nanoscale Materials at Argonne National Laboratory. Use of the Center for Nanoscale Materials was supported by the U.S. Department of Energy, Office of Science, and Office of Basic Energy Sciences under Contract No. DE-AC02-06CH11357.

■ REFERENCES

(1) Ragauskas, A.; Williams, C.; Davison, B.; Britovsek, G.; Cairney, J.; Eckert, C.; Frederick, W.; Hallet, J.; Leak, D.; Liotta, C.; Mielenz, J.; Murphy, R.; Templer, R.; Tschaplinski, T. *Science* **2006**, *311*, 484−489.

(2) Wang, H.; Male, J.; Wang, Y. *ACS Catal.* **2013**, *3*, 1047−1070.

(3) Huber, G. W.; Iborra, S.; Corma, A. *Chem. Rev.* **2006**, *106*, 4044−4098.

(4) Mohan, D.; Pittman, C. U.; Steele, P. H. *Energy Fuels* **2006**, *20*, 848−889.

(5) Oasmaa, A.; Czernik, S. *Energy Fuels* **1999**, *13*, 914−921.

(6) Maggi, R.; Delmon, B. *Biomass Bioenergy* **1994**, *7*, 245−249.

(7) Badawi, M.; Paul, J.-F.; Payen, E.; Romero, Y.; Richard, F.; Brunet, S.; Popov, A.; Kondratieva, E.; Gilson, J.-P.; Mariey, L.; Travet, A.; Maugé, F. *Oil Gas Sci. Technol.* **2013**, *68*, 829−840.

(8) Furimsky, E. *Appl. Catal., A* **2000**, *199*, 147−190.

(9) Zhao, C.; Camaioni, D. M.; Lercher, J. A. *J. Catal.* **2012**, *288*, 92−103.

(10) Zhao, C.; He, J.; Lemonidou, A. A.; Li, X.; Lercher, J. A. *J. Catal.* **2011**, *280*, 8−16.

(11) He, J.; Zhao, C.; Lercher, J. A. *J. Catal.* **2014**, *309*, 362−375.

(12) Foster, A. J.; Do, P. T. M.; Lobo, R. F. *Top. Catal.* **2012**, *55*, 118−128.

(13) Filley, J.; Roth, C. *J. Mol. Catal. A* **1999**, *139*, 245−252.

(14) Odebunmi, E. O.; Ollis, D. F. *J. Catal.* **1983**, *80*, 56−64.

(15) Nie, L.; de Souza, P. M.; Noronha, F. B.; An, W.; Sooknoi, T.; Resasco, D. E. *J. Mol. Catal. A* **2014**, *388*−*389*, 47−55.

(16) Nie, L.; Resasco, D. E. *J. Catal.* **2014**, *317*, 22−29.

(17) Kim, D. I.; Allen, D. T. *Ind. Eng. Chem. Res.* **1994**, *33*, 2942−2945.

(18) Ghiringhelli, L.; Caputo, R.; Site, L. *Phys. Rev. B* **2007**, *75*, 113403.

(19) Honkela, M. L.; Bjork, J.; Persson, M. *Phys. Chem. Chem. Phys.* **2012**, *14*, 5849−5854.

(20) Orita, H.; Itoh, N. *Appl. Catal., A* **2004**, *258*, 17−23.

(21) Hensley, A. J. R.; Wang, Y.; McEwen, J.-S. *Surf. Sci.* **2014**, *630*, 244−253.

(22) Wang, S.; Li, X.; Zhang, F.; Cai, Q.; Wang, Y.; Luo, Z. *Int. J. Hydrogen Energy* **2013**, *38*, 16038−16047.

(23) Sun, J.; Karim, A. M.; Zhang, H.; Kovarik, L.; Li, X.; Hensley, A. J.; McEwen, J.-S.; Wang, Y. *J. Catal.* **2013**, *306*, 47−57.

(24) Badawi, M.; Paul, J.-F.; Cristol, S.; Payen, E. *Catal. Commun.* **2011**, *12*, 901−905.

(25) Hensley, A. J.; Zhang, R.; Wang, Y.; McEwen, J.-S. *J. Phys. Chem. C* **2013**, *117*, 24317−24328.

(26) Hensley, A. J.; Hong, Y.; Zhang, R.; Zhang, H.; Sun, J.; Wang, Y.; McEwen, J.-S. *ACS Catal.* **2014**, *4*, 3381−3392.

(27) Hong, Y.; Zhang, H.; Sun, J.; Karim, A. M.; Hensley, A. J.; Gu, M.; Engelhard, M. H.; McEwen, J.-S.; Wang, Y. *ACS Catal.* **2014**, *4*, 3335−3345.

(28) Tereshchuk, P.; Da Silva, J. L. F. *J. Phys. Chem. C* **2012**, *116*, 24695−24705.

(29) Wang, S.; Petzold, V.; Tripkovic, V.; Kleis, J.; Howalt, J. G.; Skúlason, E.; Fernández, E. M.; Hvolbæk, B.; Jones, G.; Toftelund, A.; Falsig, H.; Björketun, M.; Studt, F.; Abild-Pedersen, F.; Rossmeisl, J.; Nørskov, J. K.; Bligaard, T. *Phys. Chem. Chem. Phys.* **2011**, *13*, 20760.

(30) Nørskov, J.; Bligaard, T.; Logadottir, A.; Bahn, S.; Hansen, L. B.; Bollinger, M.; Bengaard, H.; Hammer, B.; Sljivancanin, Z.; Mavrikakis, M.; Xu, Y.; Dahl, S.; Jacobsen, C. J. H. *J. Catal.* **2002**, *209*, 275−278.

(31) Kresse, G.; Furthmueller, J. *Phys. Rev. B* **1996**, *54*, 11169−11186.

(32) Kresse, G.; Hafner, J. *Phys. Rev. B* **1993**, *47*, 558−561.

(33) Perdew, J. P.; Jackson, K. A.; Pederson, M. R.; Singh, D. J.; Fiolhais, C. *Phys. Rev. B* **1992**, *46*, 6671−6687.

(34) Perdew, J. P.; Wang, Y. *Phys. Rev. B* **1992**, *45*, 13244−13249.

(35) Kresse, G.; Joubert, D. *Phys. Rev. B* **1999**, *59*, 1758−1775.

(36) Blöchl, P. E. *Phys. Rev. B* **1994**, *50*, 17953−17979.

(37) Klimes, J.; Bowler, D. R.; Michaelides, A. *J. Phys.: Condens. Matter* **2010**, *22*, 022201.

(38) Klimeš, J.; Bowler, D. R.; Michaelides, A. *Phys. Rev. B* **2011**, *83*, 195131.

(39) Zhong, W.; Overney, G.; Tomanek, D. *Phys. Rev. B* **1993**, *47*, 95−99.

(40) Makkonen, I.; Salo, P.; Alatalo, M.; Rahman, T. S. *Phys. Rev. B* **2003**, *67*, 165415.
(41) Herron, J. A.; Tonelli, S.; Mavrikakis, M. *Surf. Sci.* **2012**, *606*, 1670−1679.
(42) Monkhorst, H. J.; Pack, J. D. *Phys. Rev. B* **1976**, *13*, 5188−5192.
(43) Methfessel, M.; Paxton, A. T. *Phys. Rev. B* **1989**, *40*, 3616−3621.
(44) Makov, G.; Payne, M. C. *Phys. Rev. B* **1995**, *51*, 4014−4022.
(45) Jónsson, H.; Mills, G.; Jacobsen, K. W. *Classical and Quantum Dynamics in Condensed Phase Simulations*; Berne, B. J., Ciccotti, G., and Coker, D. F., Eds.; World Scientific: Singapore, 1998.
(46) Henkelman, G.; Jónsson, H. *J. Chem. Phys.* **1999**, *111*, 7010−7023.
(47) Henkelman, G.; Uberuaga, B. P.; Jónsson, H. *J. Chem. Phys.* **2000**, *113*, 9901−9904.
(48) Trygubenko, S. A.; Wales, D. J. *J. Chem. Phys.* **2004**, *120*, 2082−2094.
(49) Henkelman, G.; Arnaldsson, G.; Jónsson, H. *J. Chem. Phys.* **2006**, *124*, 044706.
(50) Laidler, K. J. *Chemical Kinetics*, 3rd ed.; Harper Collins: New York, 1987.
(51) Morin, C.; Simon, D.; Sautet, P. *J. Phys. Chem. B* **2004**, *108*, 5653−5665.
(52) Liu, W.; Ruiz, V. G.; Zhang, G.-X.; Santra, B.; Ren, X.; Scheffler, M.; Tkatchenko, A. *New J. Phys.* **2013**, *15*, 053046.
(53) Vesselli, E.; Rizzi, M.; Rogatis, L. D.; Ding, X.; Baraldi, A.; Comelli, G.; Savio, L.; Vattuone, L.; Rocca, M.; Fornasiero, P.; Baldereschi, A.; Peresii, M. *J. Phys. Chem. Lett.* **2010**, *1*, 402−406.
(54) Doronkin, D. E.; Fogel, S.; Tamm, S.; Olsson, L.; Khan, T. S.; Bligaard, T.; Gabrielsson, P.; Dahl, S. *Appl. Catal., B* **2012**, *113*−*114*, 228−236.
(55) Elahifard, M. R.; Jigato, M. P.; Niemantsverdriet, J. W. *ChemPhysChem* **2012**, *13*, 89−91.
(56) Yoon, Y.; Rousseau, R.; Weber, R. S.; Mei, D.; Lercher, J. A. *J. Am. Chem. Soc.* **2014**, *136*, 10287−10298.
(57) Brønsted, J. N. *Chem. Rev.* **1928**, *5*, 231−338.
(58) Evans, M. G.; Polanyi, N. P. *Trans. Faraday Soc.* **1938**, *34*, 11−24.
(59) Hammond, G. S. *J. Am. Chem. Soc.* **1955**, *77*, 334−338.
(60) Behtash, S.; Lu, J.; Faheem, M.; Heyden, A. *Green Chem.* **2014**, *16*, 605−616.